

BEAM DYNAMICS IN SUPERCONDUCTING PROTON LINAC*

Xin-Miao Wan, Yu-Fei Yang, Zhi-Qiang Ren, Peng-Tai Lin, Wen-Long Liao, Xiao-Bao Luo,
Xue-Jiang Pu, Zhi-Hui Li[†]

The Key Laboratory of Radiation Physics and Technology of Ministry of Education, Institute of Nuclear Science and Technology, Sichuan University, Chengdu 610065, China.

Abstract

Beam loss control is a crucial research direction in high-current superconducting linear accelerators (SCL). The research findings include firstly, for continuous beams, when tune depression (η) > 0.7 , zero current periodic phase advance (σ_{0t}) can partially exceed 90° during transport in solenoid and quadrupole doublet periodic focusing channels. Different results occur when $\eta < 0.7$. Secondly, in the solenoid system, σ_{0t} can partially exceed 90° without significant impact on beam quality. In the quadrupole doublet focusing system, the partial breakdown of 90° affects beam quality. Thirdly, Similar conclusions hold for acceleration effects. Fourthly, numerical analysis shows that double-period structures have more stringent design criteria than fully period structures. The double-period structure can cause envelope instability even if $\sigma_{0t} < 90^\circ$. Fifthly, the primary factor causing halo is the 2:1 resonance. Additionally, when η is small, higher-order resonances can also cause halo.

INTRODUCTION

Countries around the world have initiated a series of research projects related to high-power proton superconducting linear accelerators (APT, SNS, J-PARC, CADS, etc.) [1]. The understanding of beam dynamics in high-current SCL has been deepened, leading to the discovery of theories that affect the stability of beam, including envelope instability and particle-core resonance. These findings have been summarized and formulated into a set of fundamental principles for the design of SCL [2]. These principles include ensuring that the σ_{0t} is less than 90° to avoid envelope instability and prevent beam loss [3]. The first principle aims to mitigate envelope instability, while the second principle is derived from studies on halo [4]. In addition, we need to conduct systematic research on the effects of σ_{0t} exceeding 90° in the quasi-periodic focusing structure of the front section of the first acceleration stage in the SCL, as well as the halo in the double-period structure of the cryomodule with a cryostat as a unit [5].

ENVELOPE INSTABILITY

Based on the transverse motion equation, the RF electromagnetic field at the low-energy end of the linear accelerator exhibits defocusing and axial symmetry. In this study, we used a solenoid (with axial symmetry) and a non-axisymmetric quadrupole doublet as the focusing elements.

The specific parameters of these elements are shown in Fig. 1 for reference in the subsequent discussion.

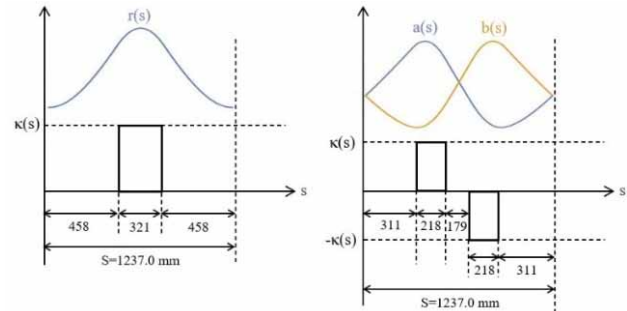


Figure 1: Periodic focusing elements and the corresponding matched beam envelopes. (a) solenoid, (b) quadrupole doublet.

We used *TraceWin* for our simulation and *PARTRAN* for multi-particle simulation and tracking. The K-V distribution and K-V envelope equations were selected for their advantages in analysing the effect of space charge. The initial kinetic energy of the proton beam was 10 MeV, and the initial normalized RMS emittance of the CW beam was $0.2 \pi \cdot \text{mm} \cdot \text{mrad}$ in both the $x-x'$ and $y-y'$ planes. A total of 100,000 particles were simulated. The envelopes where $X(s)$ and $Y(s)$ are in the two transverse directions of the periodic focusing channels are described by [6]:

$$X'' + \kappa_x(s) \cdot X - \frac{\varepsilon^2}{X^3} - \frac{2K}{X+Y} = 0 \quad (1)$$

$$Y'' + \kappa_y(s) \cdot Y - \frac{\varepsilon^2}{Y^3} - \frac{2K}{X+Y} = 0 \quad (2)$$

To study the transverse beam dynamics when σ_{0t} partially exceeds 90° , we designed five different focusing schemes for simulating σ_{0t} , as shown in Fig. 2. The maximum σ_{0t} of the beam was set to be 120° (①), 110° (②), 100° (③), and 90° (④) to observe the trend under different acceleration gradients in the presence of an acceleration field. To avoid excessive sensitivity to the focusing parameters, we generally set the minimum value of σ_{0t} to 40° after the beam passes through 80 focusing periods. Furthermore, for the case where the maximum σ_{0t} was 120° , we implemented a control scheme (⑤) to prevent envelope instability in the beam. The maximum σ_{0t} of this control scheme was set to 88° , achieved by reducing the acceleration gradient of the corresponding cavity.

* Work supported by the National Natural Science Foundation of China (Grant Nos. 11375122 and 11875197)

[†] lizhahui@scu.edu.cn

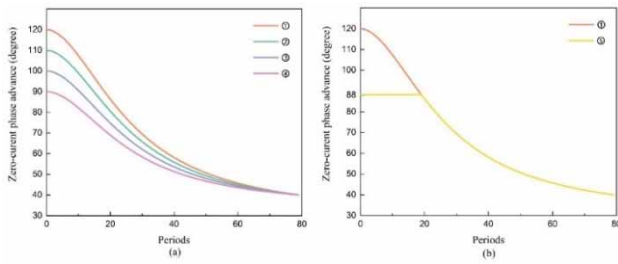


Figure 2: σ_{0t} for the five schemes. (a) Shows the focusing schemes ①-④ and (b) shows the focusing schemes ① and ⑤.

Finally, the ε of the output during beam transport was obtained, as shown in Fig. 3.

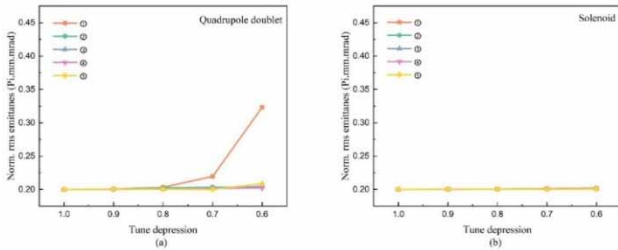


Figure 3: The ε when η was equal to 1.0, 0.9, 0.8, 0.7, and 0.6 for different focusing schemes, respectively. (a) shows that when the beams are transported in periodic focusing quadrupole doublet channels, and (b) shows that when beams are transported in a periodic focusing solenoid channel.

In Fig. 3a, it can be observed that when $\eta = 0.7$ or 0.6 , the ε value corresponding to focus scheme ① reaches its maximum. Notably, when $\eta = 0.6$, ε exceeds 10% of the initial emittance. To further analyse this phenomenon, particle distribution diagrams depicting the transportation of beams in the quadrupole doublet focusing channel under different η values are displayed in Fig. 4.

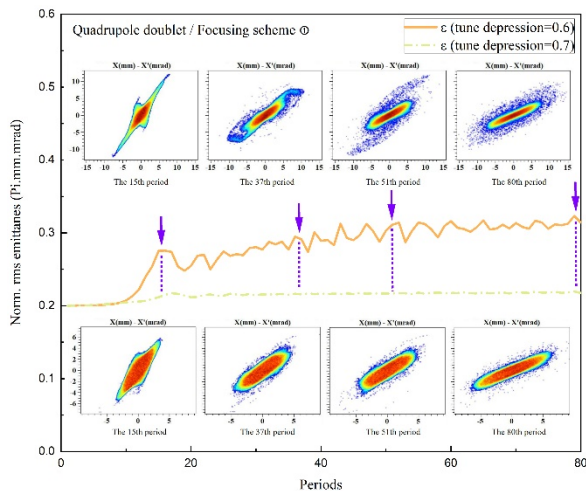


Figure 4: The ε and phase space distribution evolution along a quadrupole doublet channel under the focusing scheme ① when $\eta = 0.6$ and 0.7 , respectively. Here, the particle distribution diagrams of the 15th, 37th, 51st, and 80th periods are shown.

Based on Fig. 4, the phase space distribution of particles shows a four-fold structure and envelope instability. The 4th-order resonance occurs before the envelope instability, resulting in an overlapping region between the stopbands associated with these two instabilities. This overlap persists for a significant duration when $\eta = 0.7$ and 0.6 respectively, seeing of unstable structures in the particle phase-space distribution easier. Moreover, when $\eta = 0.6$, the beam requires more time to pass through the stopband. This suggests that the stopband has a prolonged period to attract the beam due to the space-charge effect, leading to further enhancement of the emittance. When the acceleration effect is present, it has been experimentally verified that the observed phenomena and conclusions align with those obtained in the transverse direction. And Fig. 5 shows the emittance when η is equal to 0.6 or 0.7, the ε corresponding to ① reaches maximum in quadrupole doublet.

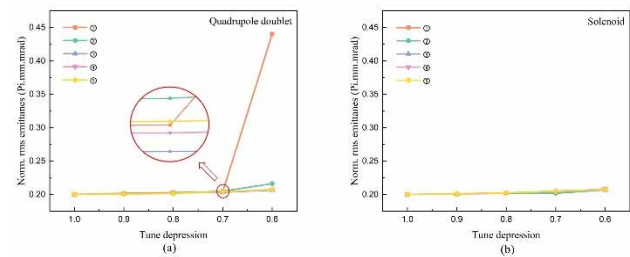


Figure 5: The ε during beam transport. (a) the ε when beams are focused by quadrupole lattices and (b) the ε when beams are focused by solenoid lattices.

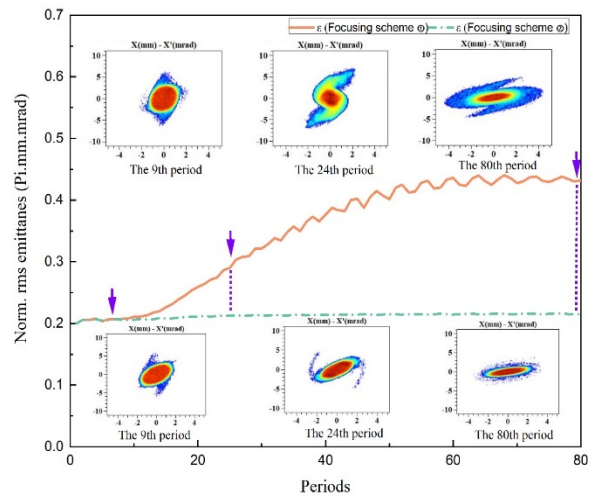


Figure 6: The ε of focusing scheme ① and ② and phase space distribution evolution along an acceleration channel that provides focusing strength by quadrupole doublet lattice when η is equal to 0.6. Here, the particle distribution diagrams of the 9th, 24th and 80th periods are shown.

In Fig. 6, it shows the corresponding particle distribution diagrams when the beam passed through 9th, 24th, and 80th periods. By comparing the results obtained by 2D simulation, ε keeps mostly consistent with it. It means that results obtained by 2D simulation can extend to 3D simulation.

HALO FORMATION IN CRYOMODULE

Obviously, in the design of cryomodule, we obtain matched envelope. To analyse the transverse motion of the beam in a double period focusing structure within a cryomodule better, we have designed the following structure as shown in Fig. 7.

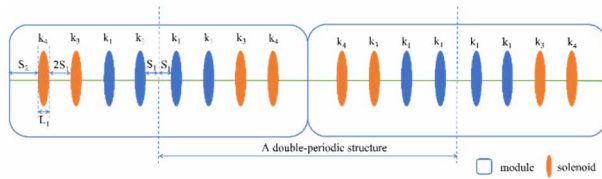


Figure 7: Double period focusing structure.

Poincare maps were computed using a double periodic structure with $s_1 = 0.25$ m, $L_1 = 0.23$ m, $s_2 = 0.63$ m, $k_1 = 13.0$ m⁻², $k_3 = k_4 = 6.0$ m⁻² and a fully periodic structure with focusing parameter k_1 as the focusing unit (slicing at the minimum of the envelope). Meanwhile, $\varepsilon = \varepsilon_x = \varepsilon_y = 0.2$ π .mm.mrad and kinetic energy is approximately 30 MeV. According to particle-core model with test particle with time follows the equation:

$$\frac{d^2x}{ds^2} + k(s)x - \frac{K}{r^2}x = 0 \quad (|x| \leq r)$$

$$\frac{d^2x}{ds^2} + k(s)x - \frac{K}{x} = 0 \quad (|x| > r)$$

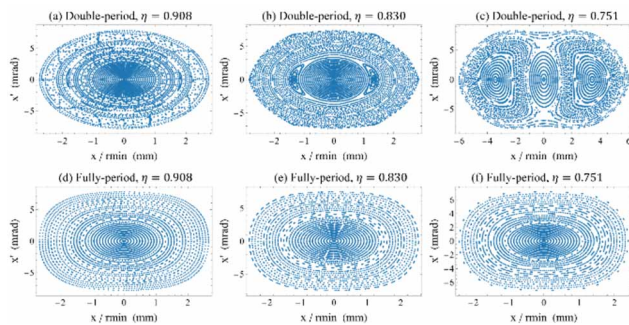


Figure 8: Stroboscopic plot for $\eta = 0.908$, $\eta = 0.830$, $\eta = 0.751$ when the beam is transported in double-period ((a), (b), (c)) and fully period ((d), (e), (f)) focusing structures respectively.

The Poincare map reflects the frequency ratio between particle and envelope oscillations. Meanwhile, the particle-core model limits the probability of particle loss. Using the double-period structure, as well as the fully periodic structure with k_1 as the period, three sets of η were set: 0.908, 0.830, and 0.751, and the Poincare maps were calculated under each of these conditions. From Fig. 8, it can be seen intuitively that the difference in the frequency ratio between particle and envelope oscillations is significant when the beam is transported in the fully periodic structure and the double-period structure. In the fully periodic structure, the frequency of the matched beam envelope oscillation is consistent with that of the particle oscillation, which is shown as circular-like ellipses on the Poincare map. In this case, we believe that there will be no beam mismatch or

beam halo. However, for the beam transported in the double-period focusing structure, it is obvious that the frequency of particle and envelope oscillations no longer remains consistent as the η decreases. The most significant change is the appearance of a prominent 2:1 resonance in the double-period focusing structure when $\eta = 0.751$, and the resonance range at 2:1 is larger at $\eta = 0.751$ than that at $\eta = 0.830$. In conclusion, from the results obtained from numerical simulations, compared with fully periodic focusing structure, the formation of beam halo is more likely to occur during beam transportation in the channel of the double-period focusing structure.

CONCLUSIONS

This study systematically investigates the envelope instability in quasi-periodic focusing structure and halo phenomena for double-periodic focusing structures in SCL. We explored the beam dynamics when σ_{0t} partially exceeded 90° for quasi-periodic structures for both 2D and 3D simulation. As for double-periodic structure, even for a matched beam, the 2:1 resonance remains a significant cause of halo formation. Furthermore, under the same beam intensity, double-periodic structures are more prone to beam halo formation compared to fully periodic focusing structures.

ACKNOWLEDGMENTS

This work was supported by the National Natural Science Foundation of China (Grant Nos. 11375122 and 11875197).

REFERENCES

- [1] Z.H. Li, P. Cheng, and H.P. Geng *et al.*, “Physics design of an accelerator for an accelerator-driven subcritical system”, *Phys. Rev. ST Accel. Beams*, vol.16, p. 080101, 2013. doi: 10.1103/PhysRevSTAB.16.080101
- [2] T. P. Wangler, K. R. Crandall, R. Ryne, and T. S. Wang, “Particle-core model for transverse dynamics of beam halo”, *Phys. Rev. ST Accel. Beams*, vol. 1, p. 084201, 1998. doi:10.1103/PhysRevSTAB.1.084201
- [3] Xin-Miao Wan, Xue-Jiang Pu, Zhi-Qiang Ren, Wei-Hong Huang, Yu-Fei Yang, and Zhi-Hui Li, “Discussion of 90° stopband in low-energy superconducting linear accelerators”, *Nucl. Sci. Tech.*, vol. 33, p. 121, 2022. doi:10.1007/s41365-022-01104-z
- [4] F.J. Sacherer, “Rms envelope equations with space charge”, *IEEE T. Nucl. Sci.*, vol. 18, pp. 1105–1107, 1971. doi:10.1109/TNS.1971.4326293
- [5] Jean-Michel Lagniel, “Chaotic behaviour and halo formation from 2D space-charge dominated beams”, *Nucl. Instrum. Methods A*, vol. 345, pp. 405-410, 1994. doi:10.1016/0168-9002(94)90490-1
- [6] J.W.G. Thomason, S.A. Fisher, D.J. Adams, M.G. Glover, J. Ranner, and D.J.S. Findlay, “Availability and reliability statistics at ISIS and at other high-power proton accelerators”, *Nucl. Instrum. Methods A*, vol. 1053, p. 168338, 2023. doi:10.1016/j.nima.2023.168338